Comput. Math. Applic. Vol. 15, No. 12, pp. 1007–1017, 1988
Printed in Great Britain.

0097-4943/88 $3.00 + 0.00

MULTIPLE SIMILARITY SOLUTIONS OF BUOYANCY INDUCED FLOWS FOR ICE MELTING IN COLD PURE WATER

C.-A. WANG and S.-J. WANG
Institute of Applied Mathematics, National Chiao Tung University, Hsinchu, Taiwan 30050, R.O.C.

(*Received* 18 *December* 1987)

Communicated by E. Y. Rodin

Abstract—A model of laminar buoyancy induced plane flows driven by the thermal transport near a vertical ice wall melting in cold pure water is studied. Computed results show that the convective inversions are found with a temperature ratio parameter R varying in [0, 1/2]. Numerical solutions are obtained in two disjoint intervals of R which are separated by a gap on which no solution exists. Multiple solutions are found at some R in these regions. With R near the lower edge of the gap, the solutions are similar. However, pairs of solutions with R varying above the upper limit of the gap are found drastically different. They indicate physically the potential existence of a large amount of energy for any trend arising that drives one flow state to another.

NOMENCLATURE

c_p—Specific heat
f—Similarity stream function
Gr_x—Local Grashof number
g—Gravitational acceleration
h_{ij}—Latent heat
Nu_x—Local Nusselt number
Pr—Prandtl number
p—Pressure
q—Exponent in density relation
R—Temperature ratio
s—Salinity
t—Temperature
u—Velocity in x-direction
v—Velocity in y-direction
W—Buoyancy function
x—Co-ordinate tangent in the ice wall
y—Co-ordinate normal to the ice wall
φ—Normalized similarity function of temperature
η—Independent similarity variable
κ—Thermal conductivity
α—Coefficient in the density correction
μ—Viscosity of fluid
ρ—Density
τ—Time
ψ—Stream function

Subscript

a—Motion of fluid
i—Quantities of ice
m—Quantities at extreme
r—Quantities at reference condition
U, L—Upper and lower solutions at the same ambient temperature or R
0—Quantities at the interface
∞—Quantities at infinity

1. INTRODUCTION

In the natural world, we frequently encounter transport processes in fluid where the motion is driven by the interface of a difference in density in the gravitational field. The occurrence of motion driving buoyancy effect may arise from a density difference caused by a temperature difference. Also, as in oceanic circulation, the difference in salinity may further affect the density differences. Therefore, the buoyancy force is the stimulus to the fluid flow, particular in oceanic circulation. All such occurrences are termed "natural convection".

The buoyancy effect arises from the action of a body force, usually gravitational, on density differences in a body of fluid. The density differences are resulted from temperature or species-concentration differences which are controlled by the nature of diffusion processes. Thus, all the diffusion may be simultaneously occurring and interacting with each other. The consequence is that all the aspects of flow and diffusive processes must be considered simultaneously. The mechanism of such flows are further complicated by the occurrence of density extreme as the temperature varies. It is known that a density extreme is reached at about 4°C in pure water at atmospheric

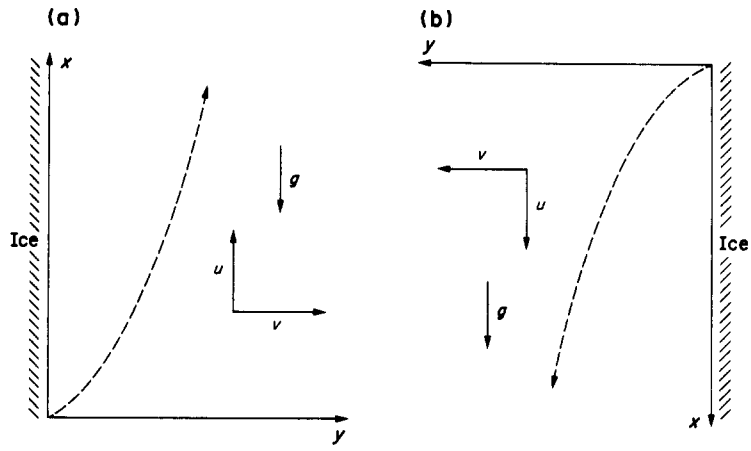

Fig. 1. Co-ordinate systems for two flow regimes: (a) the mostly upward flow and (b) the mostly downward flow.

pressure. The density extreme also occurs in saline water up to a salinity level at about 26 p.p.t. (part per thousand) and at an elevated pressure up to 300 bars absolute.

Consequently, the linear approximation of the temperature effect on density is inapplicable for water at low temperature. With data fitting, Gebhart and Mollendorf [1] have developed a new density relation for pure or saline water by imposing the temperature extreme. The formulation is very simple and accurate for convective analysis with temperature, salinity and pressure ranging from 9 to 20°C, 0 to 40 p.p.t and 1 to 1000 bars, respectively.

Moreover, Gebhart and Molledorf [2] have presented a comprehensive method with the new density formulation for analyzing convective flows in thermally buoyant pure and saline water. The results applied to the buoyancy force generated flows adjacent to a vertical surface with good agreement of experimental data of ice melting by Bendell and Gebhart [3]. In Ref. [2], a temperature ratio R has been introduced, $R = (t_\infty - t_m)/(t_0 - t_m)$, where t_∞, t_0 and t_m denote the temperature of ambient, at the vertical surface and at which the density extreme occurs. It is found that both flow and buoyancy force are upward if $R < 0$ and downward if $R > 1/2$. However, no numerical solution is obtained with R ranging from 0 to 1/2.

Recently, numbers of studies have investigated the laminar boundary layer flows in cold pure water by Carey *et al.* [4] and Carey and Gebhart [5]. For transports near the vertical isothermal surface, two distinct flow regimes, for R varying in [0, 1/2/], with local buoyancy force reversal across the thermal diffussion region have also been found by applying simple numerical schemes. The first regime is upward flow, as in Fig. 1(a), and the second regime as Fig. 1(b), is downward flow. Flows with R near 0 correspond to the first regime and those near 1/2 correspond to the latter. They also point out that the blowing effect for vertical ice melting is small and such two distinct regimes may exist.

Although the experimental work has been presented in Ref. [5], we have seen no complete computational results. It is our purpose to give a more delicate numerical study on the transports of vertical ice melting in cold pure water.

2. MODEL AND ANALYSIS

Consider a vertical wall of ice melting in pure water media. The Cartesian co-ordinate system is taken with the origin at the leading edge of ice, where the x-direction is taken positive in the direction of upstream (or downstream) and the y-direction is taken normal to the ice surface, as in Fig. 1(a) [or Fig. 1(b)]. When the co-ordinate system taken as stationary relative to the far ambient medium, the ice water interface moves in the negative y-direction with velocity $V_i(x)$ as ice melts. Thus, the flow field is time dependent and, by the order of magnitude argument, this time dependence has an effect $O(1)$ even at low ambient temperature which results in low melting rate. The Soret and Dufour effects are considered negligible.

Let u and v be the x-direction and y-direction component of fluid velocity; μ, c_p, κ and ρ_r be the absolute viscosity, specific heat, thermal conductivity and density of the convective fluid at a reference condition. Also the fluid pressure and the gravitional acceleration are denoted by p and g.

Since the boundary layer plane flows are mostly in the x-direction, therefore, the governing time dependent Navier–Stokes energy equations, due to Carey and Gebhart [6] and Gebhart and Mollendorf [1], are as follows by applying the Oberbeck–Boussinesq approximation:

$$\frac{\partial u}{\partial x}+\frac{\partial v}{\partial y}=0, \tag{1}$$

$$\rho_r\left(\frac{\partial u}{\partial r}+\frac{\partial u}{\partial x}+v\frac{\partial u}{\partial y}\right)=\mu\frac{\partial^2 u}{\partial y^2}\pm g(\rho_\infty-\rho), \tag{2}$$

$$\frac{\partial t}{\partial \tau}+u\frac{\partial t}{\partial x}+v\frac{\partial t}{\partial y}=\frac{\kappa}{\rho_r c_p}\frac{\partial^2 t}{\partial y^2}, \tag{3}$$

$$\rho=\rho_m(s,p)[1-\alpha(s,p)|t-t_m(s,p)|^{q(s,p)}], \tag{4}$$

where ρ_m is the extreme of the fluid density, t_m is the temperature at which ρ_m occures and τ denote the time. For the simplicity, the atmospheric pressure $p=1$ bar is assumed. Meanwhile, the phase change will cause the ambient fluid to move toward the ice wall with the constant velocity V_a. But both V_a and the interface velocity V_i are determined by the melting rate, and related by

$$V_a=V_i\left[1-\frac{\rho_i}{\rho_r}\right],$$

where ρ_i denotes the ice density. Moreover, V_i is assumed to be independent of time and entire ice mass is at temperature t_0. The boundary conditions, associated with equations (1)–(4), at time $\tau>0$, are at

$$y=-V_i\tau;\quad u=0,\quad v=-V_a,\quad t=t_0;\quad \text{as}\quad y\to\infty;\quad u\to 0,\quad t\to t_\infty. \tag{5}$$

Now, the boundary conditions (5) are further transformed to a fixed ice water boundary in time by letting

$$x=\bar{x},\quad y=\bar{y}-V_i\bar{\tau},\quad \tau=\bar{\tau},$$

$$u=\bar{u},\quad v=\bar{v}-V_i,\quad t=\bar{t}.$$

It is assumed that the co-ordinate system is moving with the interface, the flow field is dependent of time and $V_i^{-1}(\mathrm{d}V_i/\mathrm{d}x)$ is small and may be neglected. For the boundary layer approximation applied here, it is assumed that the convection takes place within a thin layer adjacent to $y=0$. Hence, by dropping the bars, the governing equations (1)–(3) become

$$\frac{\partial u}{\partial x}+\frac{\partial v}{\partial y}=0, \tag{6}$$

$$\rho_r\left(u\frac{\partial u}{\partial x}+\frac{\partial u}{\partial y}\right)=\mu\frac{\partial^2 u}{\partial y^2}\pm g(\rho_\infty-\rho) \tag{7}$$

$$u\frac{\partial t}{\partial x}+\frac{\partial t}{\partial y}=\frac{\kappa}{\rho_r c_p}\frac{\partial^2 t}{\partial y^2}, \tag{8}$$

with the associate boundary conditions at

$$y=0;\quad u=0,\quad v=V_0(x),\quad t=t_0,\quad \text{as}\quad y\to\infty;\quad u\to 0,\quad t\to t_\infty, \tag{9}$$

where V_0 is the blowing velocity at the interface. From the conservation of mass and thermal energy

at the interface, we have

$$V_0 = V_i \frac{\rho_i}{\rho_r} = \frac{\kappa \left.\dfrac{\partial t}{\partial y}\right|_{y=0}}{\rho_r h_{il}}, \tag{10}$$

where h_{il}, the latent heat of fusion of ice, is 79.77 cal/g.

It is clear that equation (6) implies the existence of stream function $\psi(x, y)$ which satisfies $\partial\psi/\partial y = u$ and $\partial\psi/\partial x = -v$. As in Ref. [6], a similarity variable $\eta(x, y)$, similarity function $f(\eta)$ and temperature distribution function $\varphi(\eta)$ are now defined by

$$\eta = y \cdot b(x), \tag{11}$$

$$\psi(x, y) = \frac{\mu}{\rho_r} \cdot c(x) f(\eta) \tag{12}$$

and

$$\varphi(\eta) = \frac{t(x, y) - t_\infty}{t_0 - t_\infty}, \tag{13}$$

where $c(x) = 4(\mathrm{Gr}_x/4)^{1/4} = G$ and $b(x) = G/4x$. If the local Grashof number Gr_x is defined by

$$\mathrm{Gr}_x = \frac{g \cdot \alpha(0, 1) \cdot x^3 |t_0 - t_\infty|^q \cdot p_m(0, 1) \cdot \rho_r}{\mu^2},$$

with $\alpha(0, 1) = 9.297173 \times 10^{-6}(^\circ\mathrm{C})^q$, $\rho_m(0, 1) = 9999.972\ \mathrm{kg/m^3}$, $t_m(0, 1) = 4.029325^\circ\mathrm{C}$ and $q = 1.894816$, then equations (4), (6)–(8) are transformed to the following autonomous system:

$$f''' + 3ff'' - 2(f')^2 = \pm W(\varphi, R), \tag{14$^\pm$}$$

$$\varphi'' + 3\mathrm{Pr} f\varphi' = 0, \tag{15}$$

where $W(\varphi, R = |\varphi - R|^q - |R|^q$, $R = [t_m(0, 1) - t_\infty]/(t_0 - t_\infty)$ and Pr denotes the Prandtl number with $\mathrm{Pr} = \mu \cdot c_p/\kappa$. Note that, the plus sign "+" in equation (14) is for the downward flow as Fig. 1(b) while the minus sign "−" represent the upward flows in Fig. 1(a). Furthermore, the associate boundary conditions are

$$\varphi(0) = 1, \quad \varphi(\infty) = 0$$

$$f'(0) = 0, \quad f'(\infty) = 0$$

$$f(0) = \frac{-\varphi'(0) c_p (t_0 - t_\infty)}{3\mathrm{Pr} h_{il}}. \tag{16}$$

It is clear that if (f, φ) solves the problem (14$^\pm$)–(16), then

$$\varphi'(\eta) = \varphi'(0) \exp\left[-3P_r \int_0^\eta f(s)\, \mathrm{d}s \right]$$

by integrating equation (15). Thus it can be observed that $\varphi(\eta)$ is a strictly decreasing function on $[0, \infty)$, $0 \leqslant \varphi(\eta) \leqslant 1$, and $\varphi'(\eta)$ approaches 0 as η tends to infinity. If either one of the observations fails to hold, then the boundary conditions $\varphi(0) = 1$ and $\varphi(\infty) = 0$ will be violated. Furthermore, $f''(\eta)$ can be observed to approach zero as η tending to infinity. Therefore, we have obtained two additional properties on (f, φ) which are very useful for numerical computation.

To the co-ordinate system fixed relative to the far ambient medium, the basic transport quantities, in terms of similarity variables, are related by

$$u = v \frac{G^2}{4x} f'(\eta),$$

$$-v = \frac{vG}{4x} \left\{ 3f - 3\frac{\rho_r}{\rho_i} f(0) - \eta f' \right\},$$

$$\sigma(x) = \frac{\mu v G^3}{16x^2} f''(0)$$

and

$$\mathrm{Nu}_x = -\sqrt{1/2}\varphi'(0)\mathrm{Gr}_x^{1/4},$$

where $\sigma(x)$ is the local surface shear stress and Nu_x is the local Nusselt number.

3. NUMERICAL COMPUTATIONS AND RESULTS

The boundary value problem (14)–(16) has been solved numerically by two different codes COLSYS [7] and BVPSOL [8]. In COLSYS, the method of B-spline collection at Gaussian points is implemented and a damped Newton's method is applied for the nonlinear iteration. COLSYS was choosen since the impact of spline approximation is helpful in avoiding potential difficulty caused by the lack of smoothness in the expression of the buoyancy function $W(\varphi, R)$. However, COLSYS needs a large space in core memory and, therefore, the accuracy of computed solutions is limited. In comparison with COLSYS, the multiple shooting code BVPSOL gives a modification by applying the iterative refinement sweep which is based on a perturbation analysis of the arising linear system and a rounding error analysis of the condensing algorithm. Therefore, the modification of the condensing algorithm provides the advantages of low storage requirement, without increasing mantissa length, and compensating certain typical instability.

Due to the nature of finite computation, the semi-infinite domain $[0, \infty)$ is approximated by $[0, \eta_\infty]$ with $\eta_\infty = 30, 50, 70, 110$. During the compution, solution data is said to be acceptable if the following two criteria are satisfied:

(a) values of $f''(0), -\varphi'(0)$ and $f(\eta_\infty)$ unchanged to the first five digits;
(b) the value of $f''(\eta_\infty) < 10^{-5}$.

Otherwise, we increase η_∞ with increament $\Delta\eta = 20$ until the above stopping criteria are matched. The failure of numerical computation is claimed if $\eta_\infty = 200$ is reached and one of stopping criteria fails to hold.

During the computations, COLSYS with the fifth degree B-spline function and the local accuracy parameter $\mathrm{EPS} = 10^{-6}$ is first implemented as a predictor to produce an approximation. Then, BVPSOL is imposed as a corrector by setting the local accuracy controlling parameter $\mathrm{ESP} = 10^{-8}$ to further increase the accuracy of solution data.

Table 1. Solution data at $q = 1.894816$ computed by continuation with respect to $f(\infty)$ in the region of largely upflow

R	$-\varphi'(0)$	$f(\infty)$	$f''(0)$
0.	1.041129	0.182955	0.316963
0.01008	1.0.3025	0.18	0.310459
0.040344	0.994845	0.17	0.2904118
0.065651	0.961733	0.16	0.273174
0.086630	0.931229	0.15	0.258591
0.103780	0.903606	0.14	0.246508
0.117561	0.879066	0.13	0.236725
0.128405	0.857732	0.12	0.229016
0.13672	0.839641	0.11	0.223131
0.142889	0.824735	0.1	0.218814
0.147271	0.812868	0.09	0.215804
0.150200	0.803806	0.08	0.213848
0.15199	0.797238	0.07	0.212705
0.152931	0.792799	0.06	0.212152
0.153288	0.790084	0.05	0.211988
0.153298†	0.788677	0.04	0.212039
0.153164	0.788183	0.03	0.212163
0.153037	0.788264	0.02	0.212254
0.153003†	0.788744	0.01	0.212257
0.153011	0.788969	0.0075	0.212240
0.153024	0.789357	0.005	0.212214

†Indicates the turning point.

Table 2. Solution data at $q = 1.894816$ computed by continuation with respect to $-\varphi'(0)$ in the region of largely downward

R	$-\varphi'(0)$	$f(\infty)$	$f''(0)$
0.5	0.972209	0.21733	0.177258
0.480097	0.955000	0.217343	0.160434
0.432158	0.905000	0.208362	0.117655
0.395045	0.855000	0.200684	0.081362
0.365898	0.805000	0.194047	0.049799
0.343069	0.755000	0.188367	0.021994
0.325457	0.705000	0.183629	−0.002682
0.312310	0.655000	0.179855	−0.024671
0.303014	0.605000	0.177071	−0.044306
0.297131	0.555000	0.175303	−0.061843
0.294322†	0.505000	0.174567	−0.077480
0.294336	0.455000	0.174861	−0.091363
0.297002	0.405000	0.176176	−0.103589
0.30225	0.355000	0.178497	−0.114207
0.309996	0.305000	0.181814	−0.123202
0.320409	0.255000	0.186144	−0.130484
0.333714	0.205000	0.191546	−0.135829
0.350427	0.15500	0.198183	−0.138787
0.371646	0.10500	0.206441	−0.138370
0.400223	0.055	0.217525	−0.131860
0.453983	0.005	0.238970	−0.099480

†Indicates the turning point.

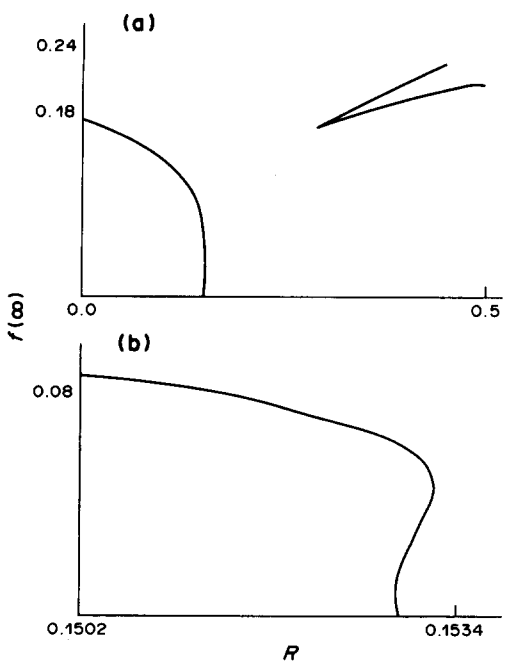

Fig. 2(a) Bifurcation diagram of parameter space of solutions in terms of R and $f(\infty)$; (b) details of $f(\infty)$ vs R in the largely upward region.

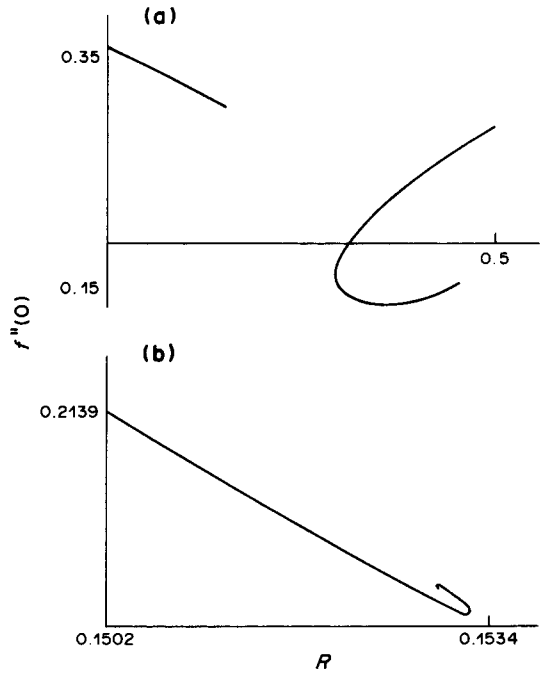

Fig. 3. (a) Bifurcation diagram of parameter space of solutions in terms of R and $f''(0)$ (the variation of the surface shear stress); (b) details of f'' vs R in the largely upward region.

By assumptions, the physical coefficients ρ_r, μ, c_p and κ are evaluated by some explicit forms at the reference condition $t = t_f = (t_0 + t_\infty)/2$, see Gebhart and Mollendorf [1], Matthaus [9], Bromley *et al.* [10] and Caldwell [11]. Moreover, the melting temperature t_0 at the interface is set to be zero in the pure water case by Fujino *et al.* [12] and Carey and Gebhart [6]. As to the Prandtl

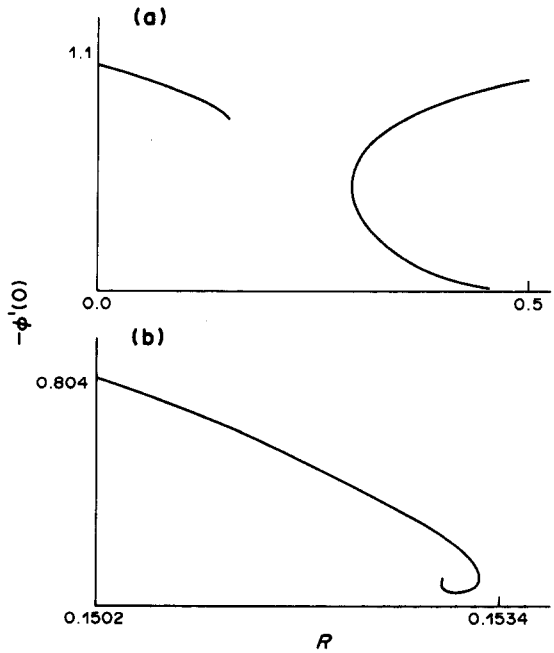

Fig. 4. (a) Bifurcation diagram of a parameter space of solutions in terms of R and $-\varphi'(0)$ (the variation of heat transfer rate); (b) details of $-\varphi'(0)$ vs R in the largely upward region.

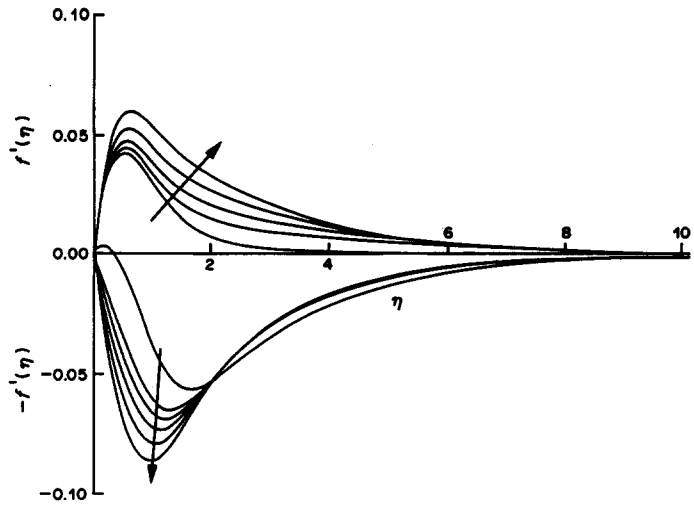

Fig. 5(a). Distributions across the flow layer of the tangent velocity angle, f' for an upward flow and $-f'$ for a downward flow. For an upflow the arrow indicates increasing R for $R = 0.065651$, 0.103780, 0.128405, 0.142889 and 0.153298. For a downflow the arrows indicates increasing R for $R = 0.297131$, 0.343069, 0.365898, 0.395045, 0.432158 and 0.480097.

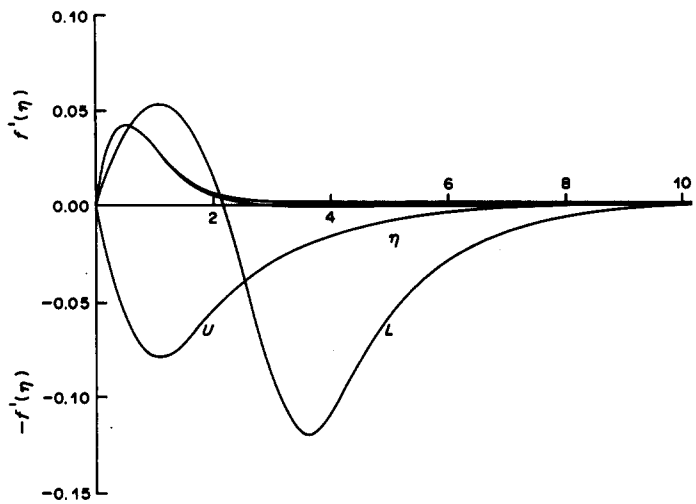

Fig. 5(b). Calculated tangent velocity profile f' in the higher and lower R regions of multiple solutions. f' for the three solutions for $R \simeq 0.153$. $-f'$ for the upper solution U at $R = 0.432157$ and lower solution L at $R = 0.453982$.

number, Pr is evaluated at reference temperature, multiple solutions are found for the parameter R ranging roughly in two regions (0.294, 0.454) and (0.1528, 0.1533). Moreover, a gap $(R_*, R^*) \approx (0.153298, 0.294322)$ is obtained on which no solution is found for the problem $(14^{\pm})$–(16). The selected values of $f(\infty)$, $-\varphi'(0)$, $f''(0)$, and R associated with the families of computed solutions are given in Tables 1 and 2. The bifurcation diagram of $f(\infty), f''(0)$ (the shear stress) and $-\varphi'(0)$ (the heat transfer rate) vs R are plotted in Figs 2–4, respectively.

As R increasing from 0.15329 [Pr = 12.355, $\varphi'(0) = -0.790067$], we find that $f'(4.2)$ first become negative at a value of R between 0.15292 and 0.15329. As R is decreasing from 0.29433 [Pr = 11.561, $\varphi'(0) = -0.455000$], we find that $f'(0.6)$ first become negative at a value of R between 0.29432 and 0.29433. Noted that the magnitude of reversals in f' increases significantly as $-\varphi'(0)$ towards 0 for $R \geqslant R^*$, whereas the magnitude of the reversal is small as $f(\infty)$ decreases towards 0 for $R \leqslant R_*$. Selected graphs of f' are plotted in Fig. 5. As mentioned earlier, the tangen velocity component $u(x, y)$, in the fixed ice water interface co-ordinate system, is proportional to the magnitude of $f'(\eta)$, then as the reversal of f' occurs, the same behavior of $u(x, y)$ is seen.

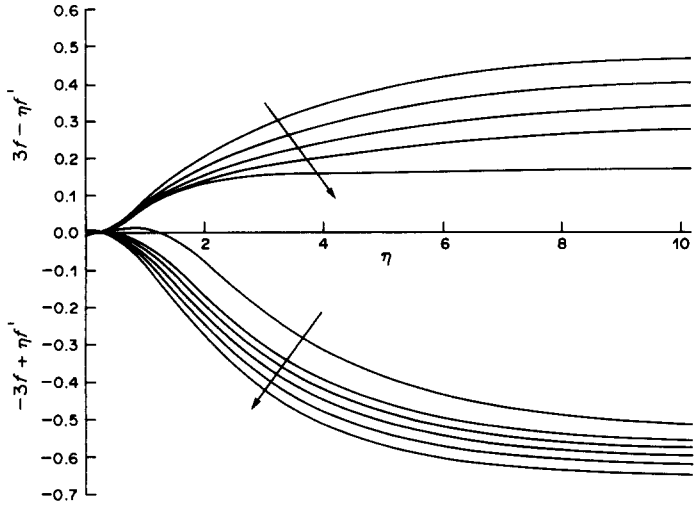

Fig. 6(a). Distributions across the flow layer of the normal velocity profile, $3f - \eta f'$ for and upward flow and $-3f + \eta f'$ for a downward flow. For an upflow the arrow indicates increasing R for $R = 0.065651$, 0.103780, 0.128405, 0.142889 and 0.153298. For a downflow the arrow indicates increasing R for $R = 0.297131$, 0.343069, 0.365898, 0.395045, 0.432158 and 0.480097.

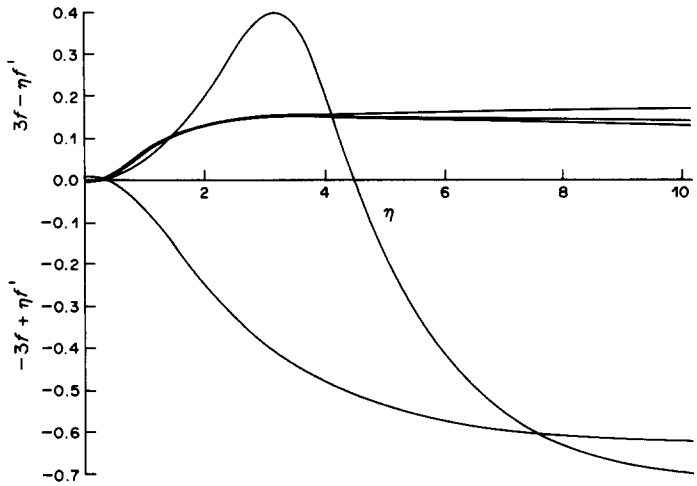

Fig. 6(b). Calculated normal velocity profile $3f - \eta f'$ in the higher and lower R regions of multiple solutions. $3f - \eta f'$ for the three solutions for $R \simeq 0.153$. $-3f + \eta f'$ for the upper solution U at $R = 0.432157$ and lower solution L at $R = 0.453982$.

Moreover, consider the normal component velocity $v(x, y)$ is fixed ice water interface co-ordinate system, which is proportional to the quantity of $3f - \eta f'$, our computations show that, as in Fig. 6, its reversal always occurs near the ice water interface for any R in $(0, R_*)$ and $(R^*, 0.5)$ and the magnitude of $3f - \eta f'$ are similar for R ranging in $(0, R_*)$. However, as also shown in Fig. 6, the behaviors of reversal for the upper and lower solutions for R ranging in $(R^*, 0.5)$ are drastically different. Furthermore, the trajectory of the temperature similarity function φ is more dramatic, which is shown in Fig. 4 for $R = 0.395045$ and $\varphi'(0) = -0.855$, we find that $\varphi(1.2) \simeq 0.1341$ and $\varphi(3) \simeq 0.61 \times 10^{-4}$, while for $R = 0.400222$ and $\varphi'(0) = -0.055$, we find that $\varphi(1.2) = 0.915265$ and $\varphi(3) = 0.168707$. The selected local surface shear stress parameter $f''(0)$, as in Fig. 7, shows another dramatic behavior, $f''(0)$ first becomes negative as R between 0.325467 and 0.343068, and as $\varphi'(0)$ towards 0 the value of $f''(0)$ becomes more negative. On the other hand, as R increases from 0 to R_* the values of $f''(0)$ doesn't become negative at all and the variation of $f''(0)$ is very slight.

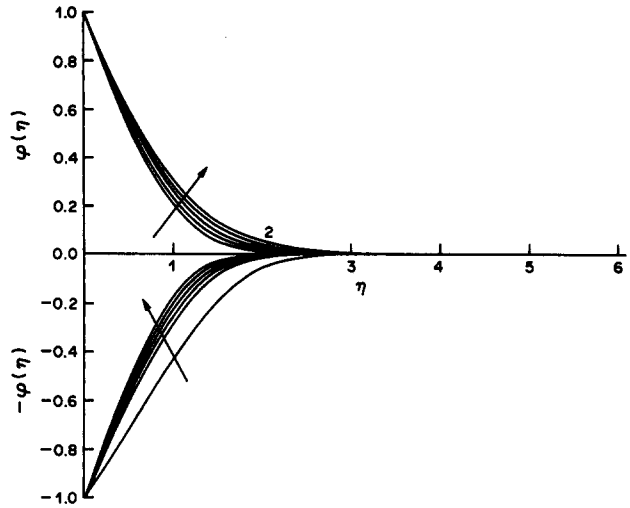

Fig. 7(a). Distributions across the flow layer of the temperature similarity function, φ for an upward flow and $-\varphi$ for a downward flow. For an upflow the arrow indicates increasing R for $R = 0.065651$, 0.103780, 0.128405, 0.142889 and 0.153298. For a downflow the arrow indicates increasing R for $R = 0.297131$, 0.343069, 0.365898, 0.395045, 0.432158 and 0.480097.

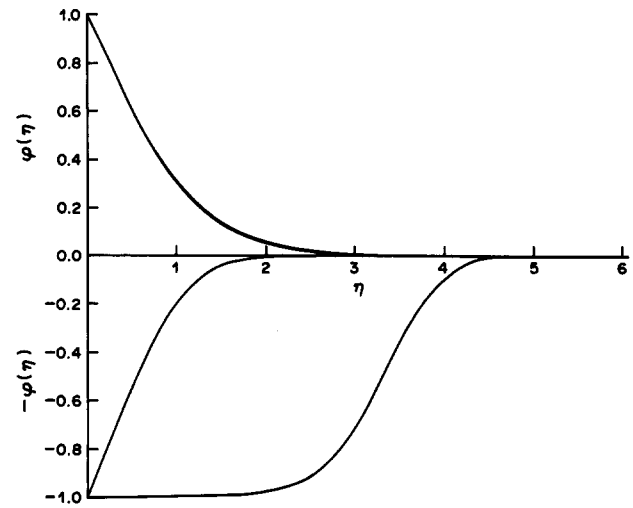

Fig. 7(b). Caculated temperature distribution φ in the higher and lower R regions of multiple solutions. φ for the three solutions for $R \simeq 0.153$. $-\varphi$ for the upper solution U at $R = 0.432157$ and lower solution L at $R = 0.453982$.

4. CONCLUSION AND FURTHER OBSERVATIONS

The gap, on which no solution is found, is roughly $0.153298 < R < 0.294322$. However, this irreducible gap is similar to the gaps obtained by the studies Carey *et al.* [4] and El-henawy *et al.* [13], although the different boundary condition (16) has been imposed, for example, the gap of R obtained in Ref [4] is (0.15, 0.29) for $\mathrm{Pr} = 11.6$ by using a usual predictor-corrector method; El-henawy [13] obtained the gap of R as (0.15181, 0.29181), for $\mathrm{Pr} = 11.6$ by using the codes: COLSYS and BOUNDS, which has narrowed the gap obtained in Ref. [7]. The finite difference method also have been applied to the time-dependent system by Wilson and Lee [14], they failed to find solutions in a slightly different gap of R on (0.111, 0.2982).

Although, all the numerical results show that there exist a gap of R, for different boundary conditions. But laboratory visualizations show that there still exist bidirectional buoyancy induced flows in these gaps [5, 15]. Observe those experimental data [5, 15] obtained in the gap. It is found that the behavior of the flows in this region are largely time-dependent effects. For instance, the

experimental data for $R = 0.254$ in Ref. [9] illustrates the sharply oscillating behavior, and unsteady behavior of the physical vertical component u at $R = 0.317$ was reported in Ref. [10]. Moreover, as time increases, the behavior is oscillating between the numerical upper solution at $R = 0.31624$ and the lower solution $R = 0.31889$ (the numerical solutions obtained by Carey *et al.* [4]). This gives a conjecture that the similarity equations can give a good measurement for the behavior of the laminar layer in the regime, which numerical solutions can be found.

By observing the bifurcation diagrams of $f(\infty)$, $f''(0)$ and $-\varphi'(0)$ against R, as in Figs 2–4, several conjectures can be made:

1. There are R_* and R^* in [0, 1/2] such that neither the problems $(14^{\pm})$–(16) has a problem for R in (R_*, R^*).
2. For R close to 0, the upward problem of problems (14^-)–(16) has a unique solution.
3. There is an $\bar{R}$ such that the upward problem (14^-)–(16) has a solution with $R = \bar{R}$ and $f(\infty) = 0$. Moreover, the problem has infinite solutions with $R = \bar{R}$.
4. For R ranging in $[R_*, 0.5)$, the downward problem $(14^+) - (16)$ has even number of solutions.

Similar phenomena had been presented for the problems of vertical ice melting in porous media by Wang [16] and the problem of isolated vertical surface in water and in porous media by El-henawy *et al.* [13] and Gebhart *et al.* [17], respectively. The conjectures for both isolated and melting cases in porous media were verified reigorously by Hastings and Karzarinoff [18] and Wang [19], respectively. However, it is still open analytically for both cases of isolated and melting surface in water.

As shown in Figs 3–5, multiple solutions in the upward flow when R is closed to R_* are very similar. Which flow might actively arise matters little in the region closed to R_*, although the existence of multiple solution means instability. However, on the other region $[R^*, 0.5)$, it is found that the lower solution exhibits a thick layer which is adjacent to the ice water interface and the thickness is increased as R increases to 1/2. Comparing the upper and lower solutions at the same R, the great differences in the temperature distribution means the huge difference of buoyancy force. This implies the potential existence of large amount of energy for amplification of disturbance from one flow state to another.

Acknowledgement—The work was supported in part by the National Science Council of the R.O.C.

REFERENCES

1. B. Gebhart and J. Mollendorf, A new density relation for pure and saline water. *Deep Sea Res.* **24,** 813–848 (1977).
2. B. Gebhart and J. C. Mollendorf, Buoyancy-induced flows in water under conditions in which density extreme may arise. *J. Fluid Mech.* **89,** 673–707 (1978).
3. M. S. Bendell and B. Gebhart, Heat transfer and ice-melting in ambient water near its density extremum. *Int. J. Heat Mass Transfer* **19,** 1081–1087 (1976).
4. V. P. Carey, B. Gebhart and J. C. Mollendorf, Buoyancy force reversals in vertical natural convection flows in cold water. *J. Fluid Mech.* **97**(2), 279–297 (1980).
5. V. P. Carey and B. Gebhart, Visualization of the flow adjacent to a vertical ice surface melting in cold pure water. *J. Fluid Mech.*, **107,** 37–55 (1981).
6. V. P. Carey and B. Gebhart, Transport near a vertical ice surface melting in saline water; some numerical computations. *J. Fluid Mech.* **117,** 379–402. (1982).
7. U. Ascher, J. Christiansen J. and R. D. Russell, COLSYS—A collocation code for boundary-value problems, notes on computer science (Ed. G. Goos and J. Hartmanis) No. 76. *Codes for Boundary—Value Problems in Ordinary Differential Equations* pp. 164–185. Springer New York (1978).
8 P. Deuflhaed and G. Bader, Multiple shooting techniques revised. Heidelberg, Technical Report Vol. 163, SFB 123, Univ. of Heidelberg (1982).
9. J. Matthaus, Die viskosita"t des Meerwassers als Funktion von Temperatur, Salzgehalt und Druck. *Mber. dt. Akad. Wiss. Ber.* **12,** (11/12), 850–855.
10. L. A. Bromley, V. A. Desaussure, J. C. Clipp and J. S Wright, Heat capacities of sea water solutions at salinities of 1 to 12% and temperatures of 2° to 80°C, *J. chem. Engng Data* **12,** (2), 202–206 (1967).
11. D. R. Caldwell, The effect of pressure on thermal and Ficckian diffusion of sodium chloride. *Deep Sea Res.* **21,** 369–375 (1974).
12. K. Fujino, E. L. Lewis and R. G. Perkin, The freezing point of sea water at pressure up to 1000 bars. *J. geophy. Res.* **79,** 1792–1797 (1974).

13. I. El-henawy, B. Hassard, N. Kazarinoff, B. Gebhart and J. Mollendorf, Numerically computed multiple steady states of vertical buoyancy-induced flows in cold pure water. *J. Fluid Mech.* **122,** 235–250, (1982).
14. N. W. Wilson and J. J. Lee, Melting of a vertical ice wall by free convection into fresh water. *J. Heat Transfer* **103,** 13–17 (1981).
15. N. W. Wilson and B. D. Vyas, Velocity profiles near a vertical ice surface melting into fresh water. *J. Heat Transfer* **101,** 313–317 (1979).
16. C. A. Wang, Multiple numerical solutions of buoyancy induced flows of a vertical ice wall melting in saturated porous media. *Comput. Math. Applic.* **14**(7), 527–540 (1987).
17. B. Gebhart and B. Hassard, S. P. Hastings and N. Bazarinoff, Multiple steady-state solutions for buoyancy-induced transport in porous media saturated with cold pure or saline water. *Numer. Heat Transfer,* **6,** 337–352 (1983).
18. S. P. Hastings and N. D. Kazarinoff, Multiple solutions for a problem in buoyancy induced flow. *Arch. ration. Mech. Analysis* **89**(3), 229–249 (1985).
19. C. A. Wang, Multiple solution of problems of ice melting in porous media. *Tamkarg J. Math.* (to appear).